Piezoelectric Unimorph Microactuator Arrays for Single-Crystal Silicon Continuous-Membrane Deformable Mirror

Yoshikazu Hishinuma and Eui-Hyeok (EH) Yang, *Senior Member, IEEE*

***Abstract*—Micromachined deformable mirror technology can boost the imaging performance of an otherwise nonrigid, lower-quality telescope structure. This paper describes the optimization of lead zirconium titanate (PZT) unimorph membrane microactuators for deformable mirrors. PZT unimorph actuators consisting of a variety of electrode designs, silicon-membrane thickness, and membrane sizes were fabricated and characterized. A mathematical model was developed to accurately simulate the membrane microactuator performance and to aid in the optimization of membrane thicknesses and electrode geometries. Excellent agreement was obtained between the model and the experimental results. Using the above approach, we have successfully demonstrated a 2.5-mm-diameter PZT unimorph actuator. A measured deflection of 5 μm was obtained for 50 V applied voltage. Complete deformable mirror structures consisting of 10-μm-thick single-crystal silicon mirror membranes mounted over the aforementioned 4×4 4 PZT unimorph membrane microactuator arrays were designed, fabricated, assembled, and optically characterized. The fully assembled deformable mirror showed an individual pixel stroke of 2.5 μm at 50 V actuation voltage. The deformable mirror has a resonance frequency of 42 kHz and an influence function of approximately 25%. [1480]**

***Index Terms*—Adaptive optics, deformable mirror, PZT actuator, space telescopes, unimorph membrane actuator.**

I. Introduction

THE need for larger aperture telescopes is driving the future trend for the development of ultralarge lightweight telescopes that can be deployed in space. Scaling up conventional, large-area, rigid, primary mirrors for space telescope applications is not a solution since launch and deployment costs are prohibitively expensive. Therefore, it is planned to construct these space-based telescopes from either smaller, mirror segments or from lightweight, large-area flexible membranes. In the latter case, the expected large surface errors could be corrected using subsequent active or adaptive wavefront control [1]. However, even the segmented-mirror approach could potentially entail wavefront errors greater than several wavelengths. Thus, there is a great need, in both cases, for efficient wavefront compensation using an optical quality, large-stroke continuous-membrane deformable mirror (DM). We propose an effective solution for this problem via our large-area high actuator density DM as shown in Fig. 1. We have successfully demonstrated that DMs with mirror surface quality of $<$10 nm can be fabricated using the membrane transfer technique first developed by our group for this application [2].

Electrostrictive lead magnesium niobate (PMN) actuators have achieved a surface stability of 0.1 nm and a surface figure of $\lambda/20$ [2]. Other materials, such as superpiezoelectric (PMN-PT) and lead zirconium titanate (PZT) ceramics, have also been developed for this application. Some of these materials have shown good cryogenic properties. However, although these technologies are in widespread use, they have only limited actuator stroke (approximately 0.5 μm stroke at 1/mm^2 actuator density, for PMN-based mirrors). Among microelectromechanical systems-based DM concepts proposed in literature, segmented deformable mirrors have been fabricated with tip/tilt capability on individual pixels [3], [4]. However, the primary drawback to these approaches is that space-based telescopes require continuous surface-figure control in order to achieve the highest possible imaging sensitivity and avoid undesirable diffraction effects arising from segmented mirror edges. Although micromachined continuous-membrane DMs have been fabricated [5]–[9], [15], such devices are based on electrostatic actuation, and consequently have limited mirror stroke (~ 2 μm). Currently, the large-aperture technology development being pursued under the recent Gossamer program has yet to demonstrate the potential for diffraction-limited wavefront quality over large apertures. Therefore, we believe that our large-actuator-stroke deformable mirror device is best suited to correct the large wavefront errors associated with space-based telescope apertures. Our unique approach of combining unimorph piezoelectric actuator technology with mirror-quality membrane-transfer technology [2] will ultimately meet the dual requirements of surface quality ($\lambda/20$ at $\lambda = 0.5$ μm) and large actuator stroke (> 6 μm at 4/mm^2 actuator density or > 30 μm at 0.1/mm^2 actuator density).

In this paper, we present the results of design, modeling, fabrication, and characterization for a set of PZT unimorph membrane actuators with various electrode designs. The work was conducted with the objective of optimizing the microactuator geometry. We also present the characterization results for a single-crystal-silicon continuous-membrane DM structure, incorporating for the first time an optical-quality mirror

Manuscript received December 10, 2004; revised August 25, 2005. This work was supported by the National Aeronautics and Space Administration and by the Jet Propulsion Laboratory under a Director's Research and Development Fund project. Subject Editor J. Judy.

Y. Hishinuma was with the Jet Propulsion Laboratory, California Institute of Technology, Pasadena, CA 91109 USA. He is now with Fuji Photo Film Co., Ltd., Kanagawa 258-8538, Japan.

E.-H. Yang is with the Jet Propulsion Laboratory, California Institute of Technology, Pasadena, CA 91109 USA (e-mail: Eui-Hyeok.yang@jpl.nasa.gov).

Digital Object Identifier 10.1109/JMEMS.2006.872229

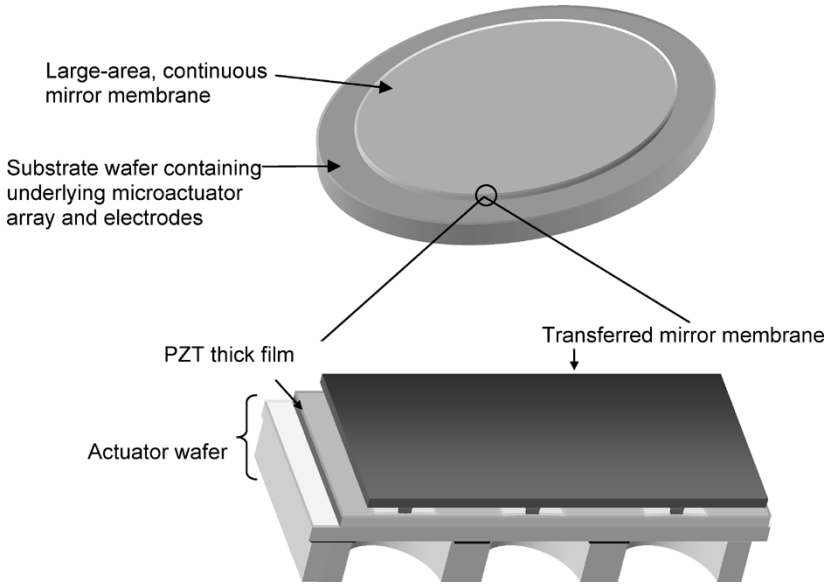

Fig. 1. Large-area continuous-membrane DM concept. The mirror membrane is mounted over an array of piezoelectric unimorph membrane microactuators. The advantage of the unimorph-membrane approach is that the small strains obtained upon application of modest voltages on the piezoelectric thin film are converted into relatively large vertical displacements.

membrane mounted over an underlying array of piezoelectric unimorph actuators.

II. PZT Unimorph Actuator-Based Deformable Mirror Concept

Our deformable mirror concept consists essentially of a continuous-membrane mirror transferred onto an underlying array of piezoelectric unimorph membrane-based microactuators. The primary benefit of the piezoelectric actuation approach is that it meets the stringent DM requirements for precision spatial control, thereby justifying the added complexity of microfabrication. Recent advances in thin-film piezoelectric material development promise to enhance the performance of these unimorph microactuators [10]. The unimorph actuation principle is illustrated in Fig. 2. The details are as follows: an electric field applied perpendicular to the membrane-mounted piezoelectric thin film induces a contraction in the lateral direction, converted by the membrane geometry to a large out-of-plane deflection. The vertical deflection acts on the portion mirror membrane mounted over the microactuator.

Compared to the conventional piezoelectric-stack actuators that are widely employed in commercial DMs, our actuation mechanism requires far less voltage and power to produce the same extent of mirror deflection. We have discovered that there are two major operating regimes for unimorph membrane actuators depending on the relative PZT film/silicon membrane thickness ratios. Actuation electrode configurations that have been tested include: full circle, concentric rings, spirals, and segmented electrodes. For thin silicon membranes (with thickness less than or equal to the PZT layer thickness), concentric rings and spiral-electrode designs produced more deflection than full-circle electrodes, implying that the stress in the electrode film reduces the amount of deflection significantly. For actuators with thick silicon membranes (thickness greater than twice the PZT film thickness), full-circle electrodes produced more deflection

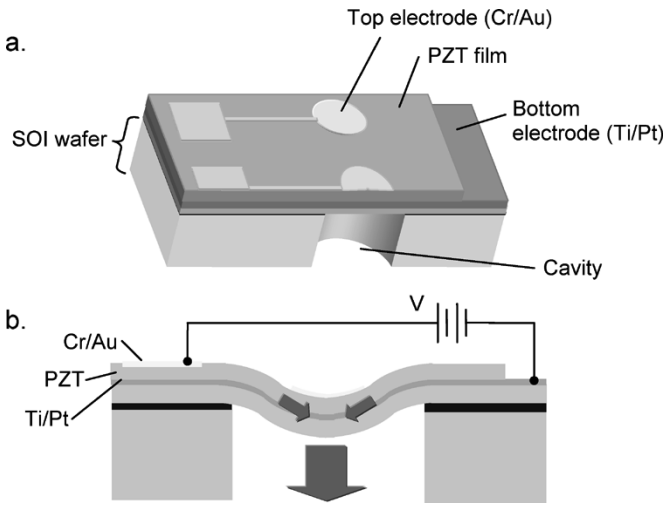

Fig. 2. Unimorph-membrane actuation principle. Voltage applied between the top and bottom electrodes sandwiching the membrane-mounted PZT thin film generates a lateral strain in the PZT film, which is converted to a vertical deflection through membrane deformation. (a) Schematic diagram showing the structure of a PZT unimorph-membrane actuator and (b) cross-sectional view of the PZT unimorph-membrane actuator.

than any of the other electrode geometries. Since actuators with thick silicon membranes showed more promise for DM applications because of the higher deflection and ease of handling during fabrication, we focused our efforts in optimizing the full-circle electrode geometry for thick silicon membranes.

III. Modeling of PZT Unimorph Actuator

In order to optimize the unimorph actuator structure, a mathematical model based on energy minimization was developed for simulating the behavior of a circular membrane with full-circle electrode geometry. This model incorporated several of the findings of Muralt *et al.* [11]. First, the following set of functions derived from the theory describing elastic behavior of thin plates

was selected as the test functions describing deflection profile of membrane:

$$w(r) = \begin{cases} \lambda\left(\frac{c_1}{4}r^2 + c_2 \ln\frac{r}{a} + c_3\right), & 0 < r < \beta a \\ \lambda\left(\frac{d_1}{4}r^2 + d_2 \ln\frac{r}{a} + d_3\right), & \beta a < r < a \end{cases} \quad (1)$$

in which r is the distance from the center of the circle, a is the radius of the membrane, $\beta{\cdot}a$ is the radius of circular electrode, and λ is the Lagrange multiplier. Six unknown coefficients are simultaneously solved by applying the appropriate boundary conditions at $r = 0$, $r = \beta \cdot a$, and for clamped edge at $r = a$. We also define the radially dependent deflection force $F(r)$ as $w(r) = \lambda \cdot F(r)$ for our convenience. The total energy of the actuator consists of three parts: U_{el} is the elastic energy of the diaphragm under deflection, U_M is the potential energy due to bending moment of piezoelectric film, and U_S is the stretching energy due to the tensile film stresses. These energy terms are given by

$$\begin{aligned} U_{el} &= \frac{1}{2}D\lambda^2 \int_0^a 2\pi r \left[\left(\frac{d^2F}{dr^2} + \frac{1}{r}\left(\frac{dF}{dr}\right)\right)^2 \right. \\ &\qquad \left. -2(1-\nu)\frac{1}{r}\frac{dF}{dr}\frac{d^2F}{dr^2}\right] dr \\ U_s &= \frac{1}{2}S\lambda^2 \int_0^a 2\pi r \left(\frac{dF}{dr}\right)^2 dr \\ U_M &= \frac{1}{2}M\lambda \int_0^{\beta a} 2\pi r \left(\frac{d^2F}{dr^2} + \frac{1}{r}\frac{dF}{dr}\right) \end{aligned} \quad (2)$$

where D is the flexural rigidity of the circular membrane given by

$$D = \frac{Yh^3}{12(1-\nu^2)} \quad (3)$$

where Y is the Young's modulus, h is the thickness of the membrane, and ν is the Poisson's ratio. The S in U_s is the stretching "spring constant" (force per unit length), given by

$$S = S_p + S_f = \beta\sigma_p t_p + \sum \sigma_i \cdot t_i, \quad (4)$$

where σ_p is the PZT stress generated in lateral direction, t_p is the thickness of the PZT film, and σ_i is the stress in the ith film of thickness t_i. The factor β is the ratio of the circumferences of the actuator electrode and the membrane. The bending moment M is obtained as

$$M = \sigma_p t_p \frac{h_{\text{eff}}}{2} \quad (5)$$

where $h_{\text{eff}}/2$ is the effective distance between the center of the PZT film and the neutral plane (zero strain plane) of the actuator membrane. The total energy of the membrane under deflection is therefore

$$\begin{aligned} U_{tot} &= U_{el} + U_s + U_M \\ &= \frac{1}{2}D\lambda^2 a^2 N_{el}(1,\beta) + \frac{1}{2}S\lambda^2 a^4 N_s(1,\beta) \\ &\quad + \frac{1}{2}M\lambda a^2 N_M(1,\beta) \end{aligned} \quad (6)$$

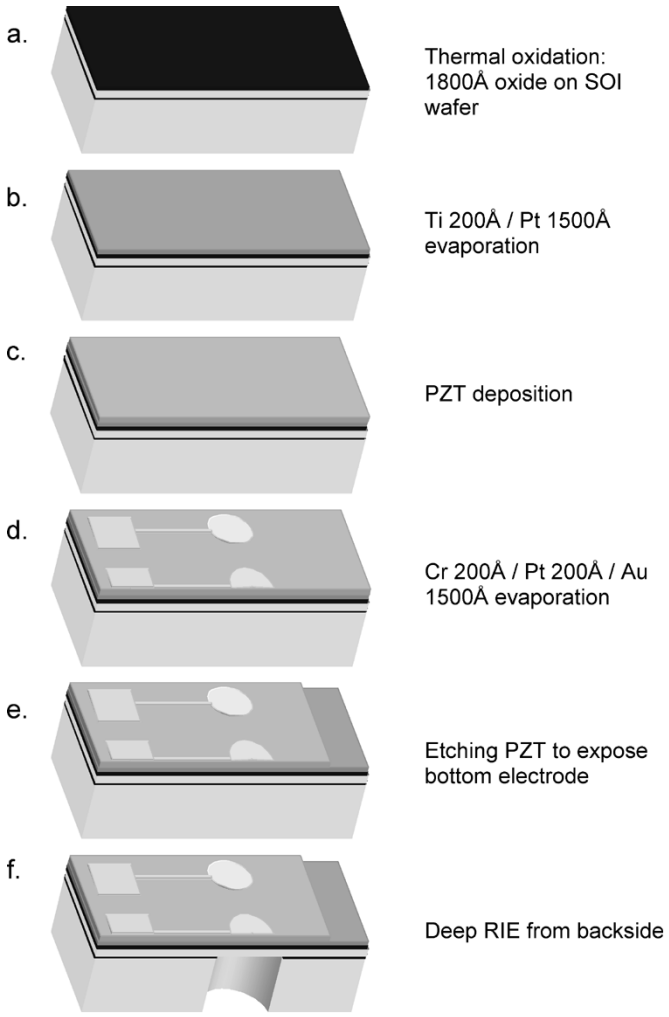

Fig. 3. Fabrication sequence for the PZT unimorph actuator. (a) An SOI wafer was thermally oxidized. (b) Ti 20 nm/Pt 150 nm layers were evaporated on the front surface of the SOI wafer. (c) Thin ($\sim$ 2 μm) PZT films were prepared using a sol-gel deposition process. (d) Cr 20 nm/Pt 20 nm/Au 150 nm layers were evaporated onto the PZT layer and patterned to form top electrodes and contact pads. (e) A two-step wet-etching process for PZT thick films was used to expose the bottom electrode. (f) Backside cavities were formed by DRIE until the SOI buried oxide was exposed. After the buried oxide was removed in BOE, further reactive ion etching was performed to thin down the silicon membrane as needed.

where $N_{\#}(1,\beta)$ are integrations in (2) evaluated at $a = 1$. The energy minimization condition $\partial U_{tot}/\partial\lambda = 0$ yields

$$\lambda_{\min} = -\frac{\frac{1}{2}N_M(1,\beta)M}{N_{el}(1,\beta)D + N_s(1,\beta)a^2 S}. \quad (7)$$

Hence, the center deflection of the diaphragm is obtained as

$$w(0) = \lambda_{\min}F(0) = 2\ln 2 \cdot a^2\lambda_{\min}. \quad (8)$$

According to this model, maximum deflection occurs at an intermediate membrane thickness. This thickness depends on piezoelectric film thickness, piezoelectric stress coefficient (e_{31}), and residual stresses in the thin films comprising the membrane. For this calculation we used values of $t_p = 2\ \mu$m, $e_{31} = -6$ C/m^2, and film stress parameters independently determined from film stress measurement optical measurements.

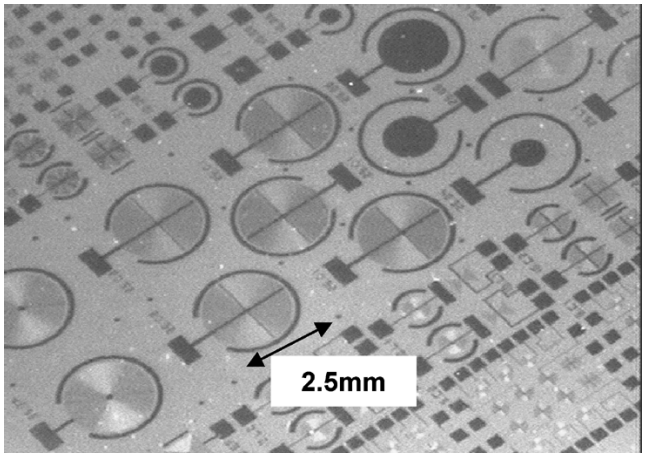

Fig. 4. Photograph of various types of PZT unimorph actuators fabricated on a single wafer. There are two types of geometries for unimorph-membrane actuators depending on the PZT film/silicon membrane thickness ratio. For thin silicon membranes (less than or equal to the PZT-layer thickness), concentric-rings and spiral-electrode geometries produced more deflection than full-circle electrodes, implying that the stress in the electrode film reduces the amount of deflection significantly. For actuators with thick silicon membranes (greater than twice the PZT thickness), full-circle electrodes produced more deflection than the other electrode designs. Since actuators with thick Si membranes showed more promise for DM applications because of the higher deflection and ease of handling during fabrication, we focused our efforts in optimizing the full-circle actuator design for thick Si membranes.

IV. Fabrication of Actuators and Mirrors

A. Piezoelectric Unimorph Actuators

The fabrication sequence for unimorph actuators is schematically depicted in Fig. 3. A silicon-on-insulator (SOI) wafer was thermally oxidized [see Fig. 3(a)]. $\mathrm{Ti}(200\ \text{Å})/\mathrm{Pt}(1500\ \text{Å})$ layers were subsequently evaporated on the front surface of the SOI wafer [see Fig. 3(b)]. Then, thick ($\sim 2\ \mu$m) PZT films were prepared using a sol-gel deposition process (the PZT films were prepared at Pennsylvania State University) [see Fig. 3(c)]. $\mathrm{Cr}200\ \text{Å}/\mathrm{Pt}\ 200\ \text{Å}/\mathrm{Au}\ 1500\ \text{Å}$ layers were evaporated onto the PZT layer and patterned to form top electrodes and contact pads [see Fig. 3(d)]. A two-step wet-etching process for PZT thick films was used to expose the bottom electrode [see Fig. 3(e)] [11]. For the deep reactive ion etching (DRIE) process, a dental wax was coated on a dummy wafer at 130 °C after patterning the backside of the wafer. The wafer was mounted on the dummy wafer prior to the DRIE process. Finally backside cavities were formed by DRIE until the buried oxide was exposed [see Fig. 3(f)]. After the buried oxide was removed in buffered oxide etchant (BOE), further reactive ion etching was performed to thin down the silicon membrane as needed. The wax-covered PZT and metal layers were not exposed to the following etching process. Four different silicon membrane thicknesses per wafer were created using the Kapton tape-based masking approach, which covered some of the wafer areas for selective etching of the cavities by $5 \sim 10\ \mu$m, after the major DRIE process was completed [12]. Fig. 4 contains optical micrographs of various actuator geometries fabricated on the same wafer.

B. Mirror Membrane and Bonding

DMs consisting of 10-μm-thick single-crystal silicon membranes supported by 4×4 actuator arrays were fabricated and assembled. The fabrication sequence of a mirror membrane fabricated from an SOI wafer is illustrated in Fig. 5. The windows for electrode pads were patterned and etched [Fig. 5(a)]. After patterning the backside, the wafer was wax-mounted on a dummy wafer at 130 °C for the DRIE process. The wafer substrate was etched using DRIE from the backside to define membrane windows, creating the individual mirror membranes [Fig. 5(b)]. The buried oxide of the SOI wafer was etched right after the DRIE process while the wafer was mounted on the dummy wafer. A Cr/Pt/Au multilayer sandwich was evaporated and patterned followed by the deposition of a 2-μm-thick indium (In) layer on the patterned photoresist exposing the Au bonding pads. Since In only adheres to the Au layer and not the thermal oxide, the Au pad "localizes" the In deposit for subsequent thermocompression bonding. Also, In oxidizes instantly when exposed to air and hinders bond formation. As an oxidation preventive measure, a 10-nm-thick Au layer was deposited in situ, thus "capping" the In surface. A similar metallization scheme was also used for the actuator wafer [Fig. 5(c) and (d)]. Finally, the two wafers were aligned and bonded by thermal compression [Fig. 5(e)]. A Karl Suss aligner and thermocom-

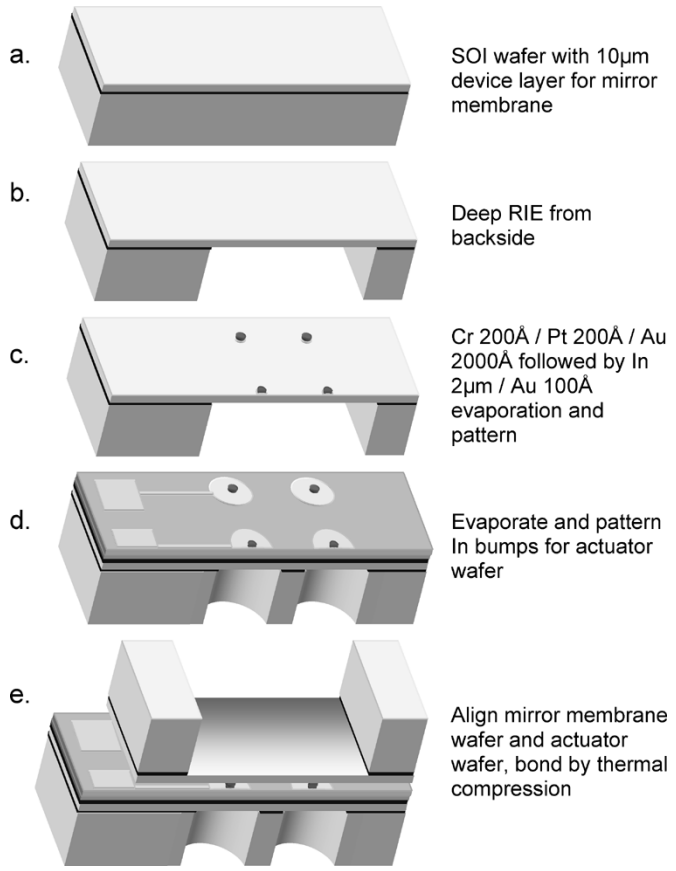

Fig. 5. Fabrication sequence for mirror-membrane wafer and deformable mirror assembly. (a) The mirror membrane is fabricated from a SOI wafer. (b) The SOI substrate is etched away completely using DRIE from the backside in order to define the membrane windows, creating the individual mirror membranes. (c), (d) Following the deposition and patterning of a Cr/Pt/Au multilayer stack, a 2-μm-thick indium (In) layer is then deposited by thermal evaporation, after patterning photoresist to expose Au bonding pads. These deposited In/Au layers for bonding are subsequently defined using a liftoff process on both the mirror-membrane and actuator wafers. (e) The two wafers are aligned and bonded by thermal compression.

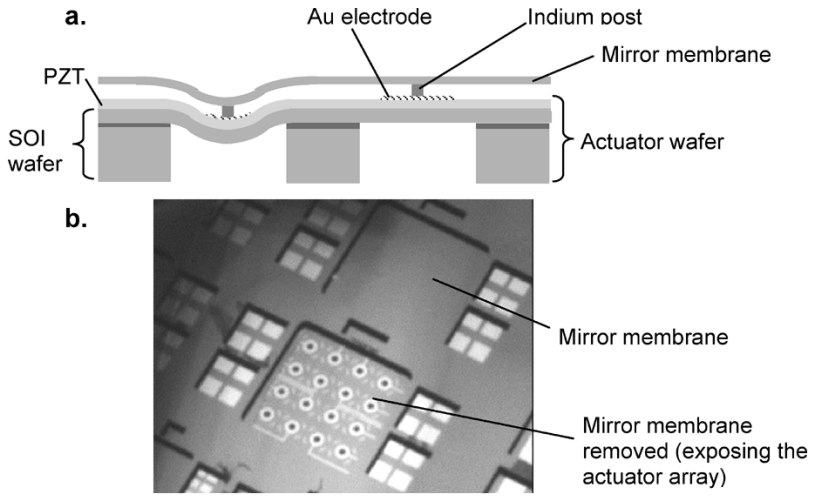

Fig. 6. Assembled DM device with 4 × 4 unimorph actuator array. (a) Cross-sectional schematic of the deformable mirror. (b) SEM micrograph of microfabricated deformable mirrors with 4 × 4 actuator arrays.

pression bonder were used to align and bond the two wafers. The bonding chamber was evacuated to a pressure of 1×10^{-5} torr prior to the bonding operation. Thermocompression bonding of the two wafers was conducted using a piston pressure of 100 kPa applied at 153 °C. From PZT actuator membrane and silicon mirror membrane stiffness calculations, the estimated force applied to the center of an actuator membrane during bonding is on the order of a few millinewtons. Fig. 6 contains (a) a cross-sectional schematic diagram of the DM structure and (b) a micrograph of DMs and the microfabricated arrays of actuators (the upper mirror membrane is intentionally removed). SEM micrographs of the fabricated DM structure are shown in Fig. 7.

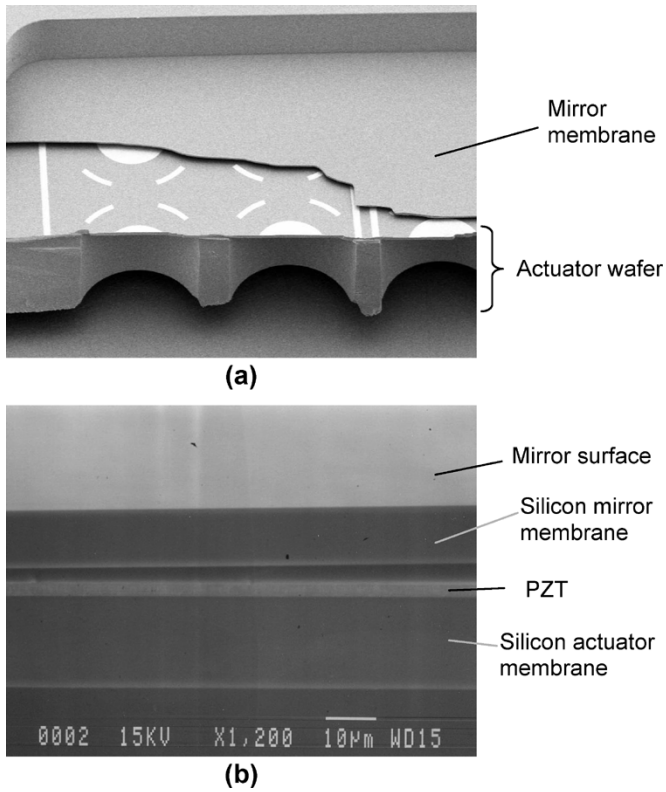

Fig. 7. SEM micrographs of the assembled deformable mirror. (a) DM with mirror membrane partially removed. (b) Cross-sectional view of the DM.

V. Optical Characterization

A. Actuation of Piezoelectric Unimorph Actuators

A WYKO RST Plus Optical Profiler was used to analyze the deflections of the actuator membranes. The deflection behavior of a typical unimorph actuator device is shown in Fig. 8. The measured surface roughness of our typical PZT film is approximately 10 nm. Fig. 9 contains deflection measurements of a unimorph actuator as a function of voltage, showing a typical hysteresis loop for a piezoelectric actuator. In order to maximize the deflection, unimorph actuators with different silicon membrane thicknesses were characterized. Actuators with different membrane thicknesses were obtained on the same wafer by selectively etching the silicon membrane to different final thicknesses using the Kapton tape-masked backside etching process described above. The actuation results for the cases of 1) 2.5 mm and 2) 1.0 mm membrane diameters with 60% electrode coverage and a 2-μm-thick PZT film are shown as a function of the membrane thickness (Fig. 10). The experimental results are superimposed over their respective predicted deflection curves from the simulation model. As predicted by our model, the maximum deflections were obtained at intermediate silicon-membrane thicknesses of 1) 15 μm for the 2.5-mm-diameter and 2) 7 μm for the 1.0-mm-diameter actuator. Also, actuators with several different top electrode sizes relative to the membrane diameters were fabricated and tested. It was found that an electrode diameter that is approximately 60% of the membrane diameter produces the most deflection for the case of the 2 μm PZT/15 μm silicon membrane combination (Fig. 11). The stroke of the mirror depends on the thickness of the mirror membrane. Further optimization must be done by adjusting the thickness of the mirror, PZT, and actuator membranes. In addition, the piezoelectric coefficient of the PZT-film can be increased by improving the PZT-film formation process.

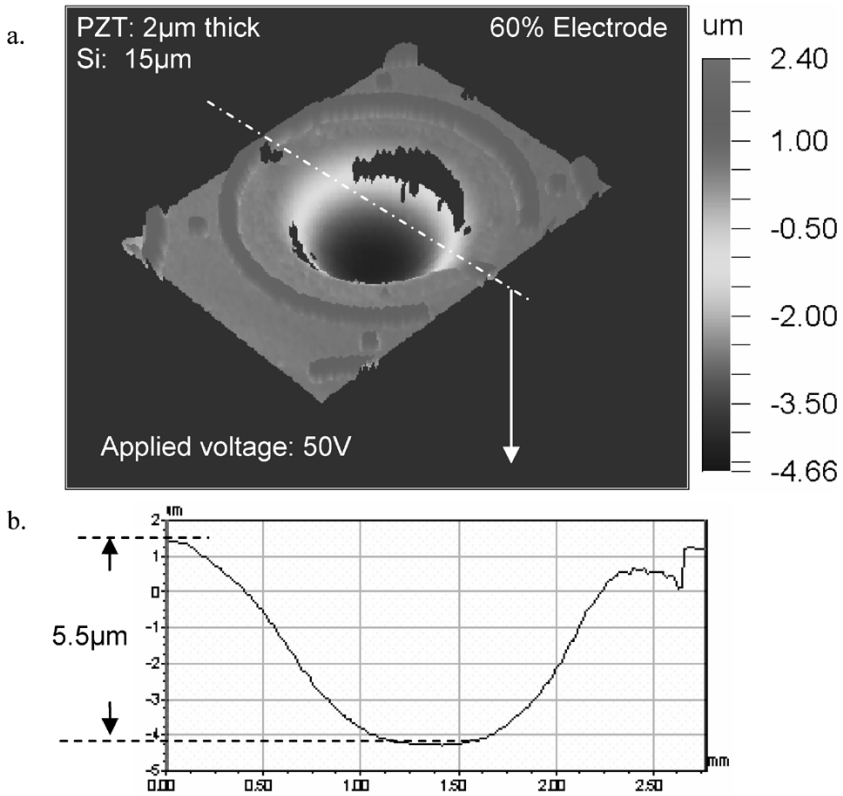

Fig. 8. WYKO Optical profiler image of the PZT unimorph actuator under deflection.

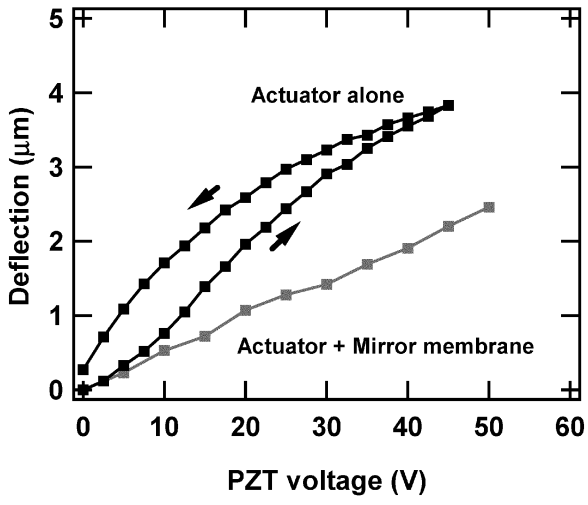

Fig. 9. Deflection (stroke) versus voltage for the actuator with or without an overlying mirror membrane. A 2.5-mm-diameter actuator had a stroke of $\sim$ 4 μm at 45 V. The stroke was reduced for a fully assembled deformable mirror to approximately 2.5 μm at 50 V.

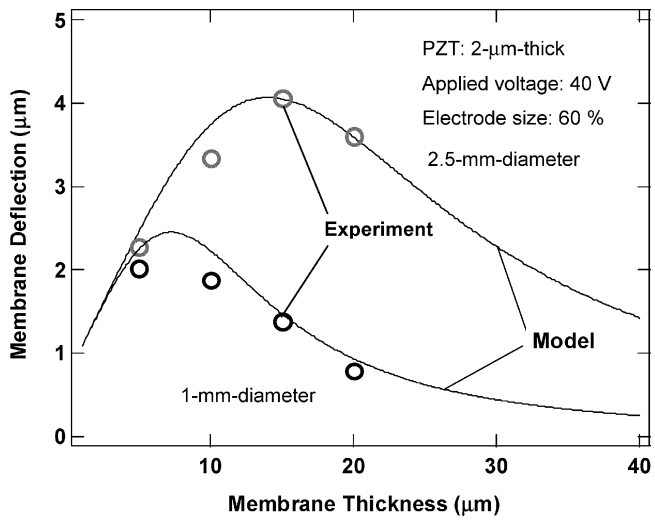

Fig. 10. Dependence of actuator deflection on the thickness of the silicon membrane. For 2.5-mm-diameter membranes, the optimized Si/PZT thickness ratio was approximately six. The data points represent an average of ten separate measurements on two different pixels within a typical actuator array.

B. Deformation of Mirror Membrane

DMs consisting of 10-μm-thick single-crystal silicon membranes supported by 4 $\times$ 4 actuator arrays were characterized optically. Fig. 12 contains an optically measured surface profile for an as-transferred mirror membrane with an area of 3 $\times$ 6 mm, showing a root-mean-square roughness of about 26 nm. Although the mirror surface was not coated with any materials in this paper, an optical coating will ultimately be required to enhance the reflectivity. The surface profiles of the actuated deformable mirror using the underlying actuators are shown in Fig. 13. The print-through can be minimized by using thicker mirror membrane with a reduced mirror deflection. The print-

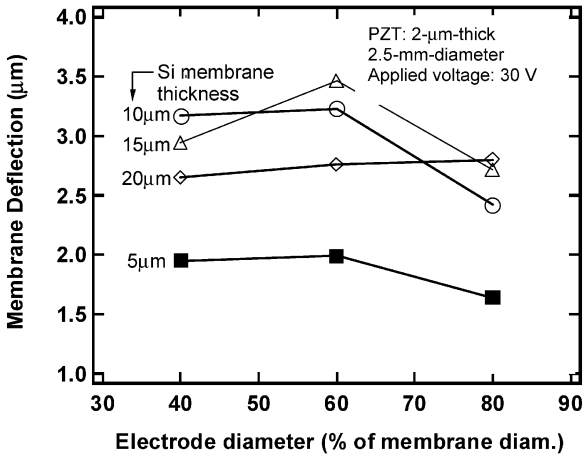

Fig. 11. Dependence of actuator deflection on the electrode diameter expressed as a fraction of the membrane diameter. The optimum electrode diameter is approximately 60% of the membrane diameter.

through can also be further reduced, by using silicon posts instead of indium posts. The measured influence function is approximately 25%. Influence function refers to the interactuator coupling or cross-talk between adjacent pixels.

The DM has a stroke (deflection) of 2.5 μm at an actuation voltage of 50 V. The stroke of the mirror membrane is approximately 40% less than that for the actuator alone (Fig. 9). The full scale measurement (up and down) of the mirror and actuator combination was not performed, due to a lack of reference area on the mirror membrane. Hence, the measurements on the mirror membrane were made in the "differential mode" only. For the actuator alone, the measurements were made with respect to reference electrodes. This stroke reduction can be adjusted by varying the mechanical compliance (by optimizing the PZT/actuator membrane/mirror membrane thickness ratio). The frequency responses for the unimorph actuator, with and without the mounted mirror membrane, were obtained using a laser-doppler vibrometer (shown in Fig. 14). The resonance frequency of a 2.5-mm-diameter 2 μm PZT/15 μm Si and 60% electrode actuator was measured at 47 kHz, which far exceeds the bandwidth requirement for most DMs (sim1 kHz). Deformable mirror bandwidth is important for adaptive optics applications, where the time scale for aberration fluctuations is on the order of a few milliseconds. The mirror response should not contribute to the latency of the control system. Therefore, mirror shape should be controlled at a speed faster than that of the changing aberration [13].

VI. Discussions

The inherent hysteresis problem for PZT actuators leads to the problem that deflections obtained at a particular actuation voltage can vary depending on whether the new actuation voltage was applied during a ramp up or a ramp down from the previous state. One approach to mitigate the hysteresis problem for open-loop control is to choose to stay on the same segment (either ramp up or ramp down) of the hysteresis loop for all actuation voltages. This is possible because the bandwidth of our PZT actuator far exceeds the requirement of the DM bandwidth ($\sim$1 kHz). For instance, if the maximum voltage swing for the actuator is from 0 to 50 V and if we choose to be on the ramp-up segment of the hysteresis loop, then in order to reduce the actuation voltage from, say, 30 to 20 V, we can first ramp down the voltage up to 0 V and then ramp back up to 20 V, instead of directly ramping down to 20 V. Since the direct piezoelectric coefficient is frequency dependent [14], actuating the membrane too quickly is undesirable.

The strategy of staying on one side of the hysteresis loop does not completely eliminate hysteresis; it does, however, reduce it significantly. In general, three schemes are possible to solve the problem. The first scheme is to always approach a set-point from the same direction and the same extreme, before tracing out the whole hysteresis loop every time. This approach does not require feedback signal and computation, but it must go to the limit of the actuator range every time a setting is changed. Therefore, it is not suitable where the wavefront requires continuous adjustments at high rates. The second scheme is to perform closed-loop control, which requires an independent position reference, either from a capacitive displacement measurement or from an optical wavefront sensor. This method is fast and simple in control but needs independent position measurement for control. The third scheme is to use open-loop predictive control based on actuator history. This scheme keeps a material hysteresis model in software and updates the "poling" state of the material, based on the history of actuation. Therefore, no feedback signal is needed, enabling a "continuous sensing" mode (such as atmospheric turbulence compensation). The disadvantage of this approach is that it requires more computation, which may not be suitable where a large number of actuators are used at high update rates due to prohibitively long computation times.

VII. Conclusions

We have described the design, modeling, fabrication, assembly, and testing of large-stroke piezoelectric unimorph actuators for deformable mirror applications. We have successfully demonstrated a proof-of-concept DM composed of a continuous single-crystal-silicon membrane supported by piezoelectric unimorph actuator arrays. Piezoelectric unimorph actuators designed with optimized PZT/Si thicknesses can produce a stroke as high as 5 μm at an actuation voltage as low as 50 V. DMs consisting of 10-μm-thick single-crystal-silicon membranes supported by 4 $\times$ 4 actuator arrays were fabricated and characterized optically. Improvements in the fabrication process for better optical-quality mirror membranes and optimization of the DMs for larger strokes are under way. Additional optical characterization of the fully assembled DMs will also be performed. The deformable mirror concept described in this paper will support the requirements of several future space missions. The MEMS-based large-stroke actuator technology described here is a new capability that is expected to benefit future space missions that require precision miniature devices in a broad range of operational environments. The development path for this novel technology includes verification

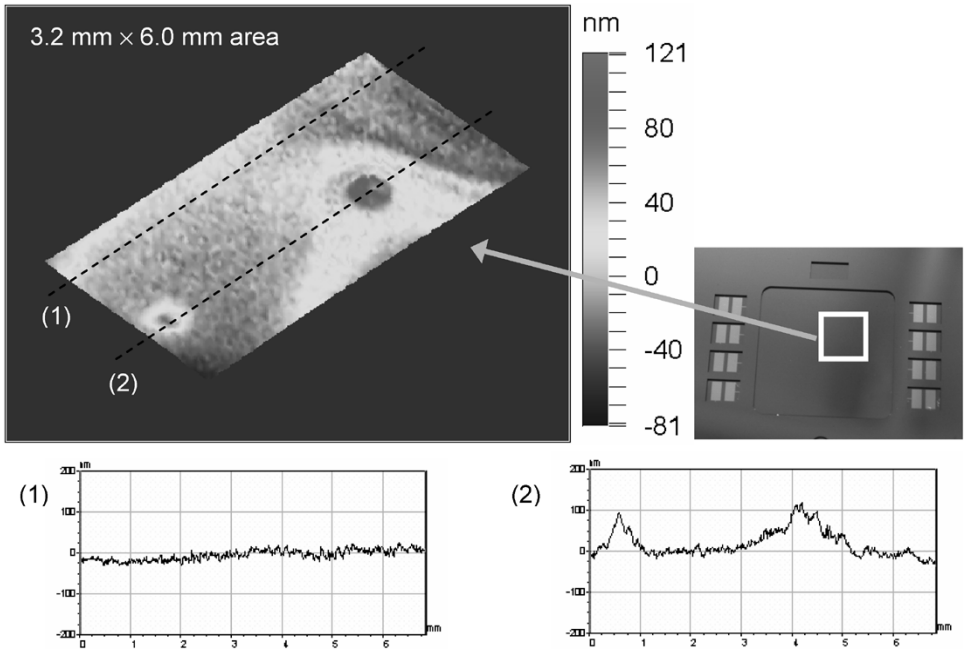

Fig. 12. Initial surface figure of the as-assembled DM with 4 × 4 actuators. The surface-figure error (mirror surface height variation) was approximately 26 nm. The major asperities are caused by the "print-through" from the indium bumps used to bond the mirror membrane to the individual underlying actuators.

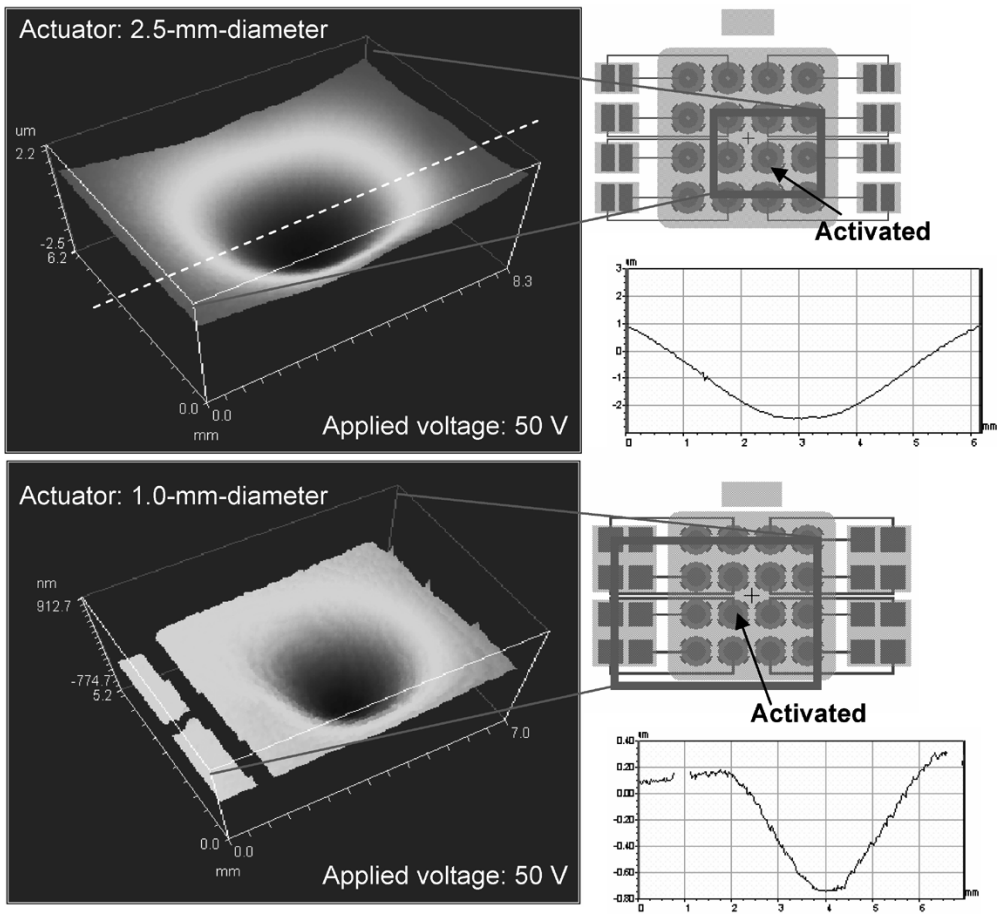

Fig. 13. Optically measured deflection profile for the assembled deformable mirror under the actuation of 2.5-mm-diameter actuators. From these profiles, the influence function ("crosstalk" deflection at pixels adjacent to the actuated pixel) was measured to be approximately 25%.

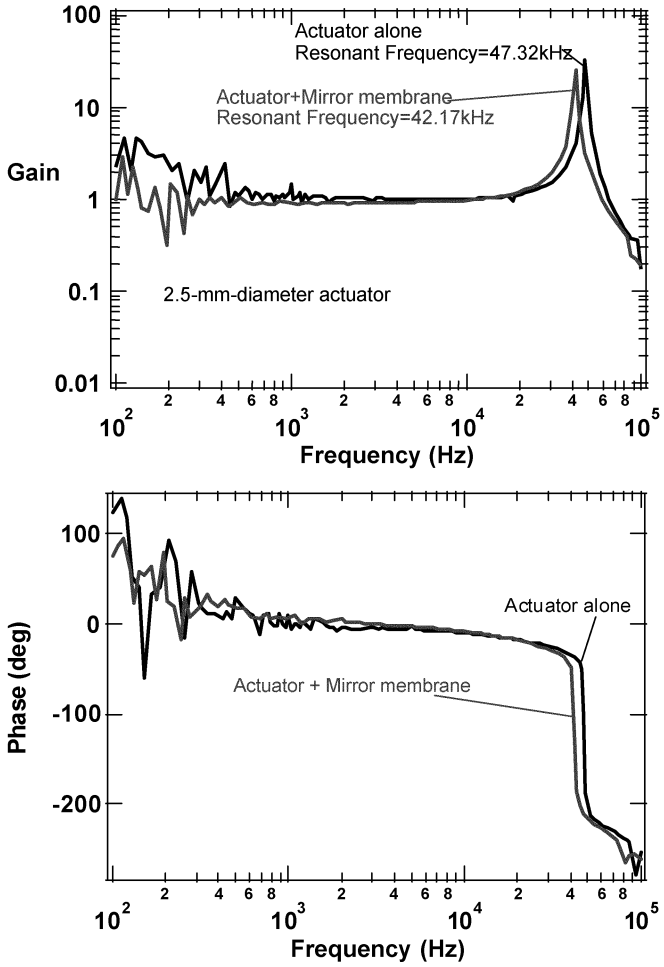

Fig. 14. Measured frequency response of the piezoelectric unimorph actuator with and without a mounted mirror membrane. The frequency responses show that the fully assembled DM is capable of high bandwidth operation.

of performance on ground-based telescopes, diffraction-limited imaging systems, and laser-based communications systems.

ACKNOWLEDGMENT

The authors would like to thank Dr. J.-G. Cheng and Prof. S. Trolier-McKinstry at Pennsylvania State University for performing the PZT deposition on our silicon wafers. The authors also would like to thank Dr. B. M. Levine and Dr. E. Bloemhof at the Jet Propulsion Laboratory for their technical and programmatic support. They would like to acknowledge Dr. T. George and Dr. K. Shcheglov for their valuable comments throughout this research project.

REFERENCES

[1] R. G. Dekany, D. G. MacMartin, S. Padin, G. A. Chanan, and M. Troy, "Advanced Segmented Silicon Space Telescopes (ASSiST)," in *Proc. SPIE Int. Symp. Astronomical Telescopes and Instrumentation, Adaptive Optical System Technologies II*, Waikoloa, HI, 2002.

[2] E. H. Yang and D. V. Wiberg, "A wafer-scale membrane transfer process for the fabrication of optical quality, large continuous membranes," *J. Microelectromech. Syst.*, vol. 12, no. 6, p. 804, 2003.

[3] V. M. Bright, J. H. Comtois, J. R. Reid, and D. E. Sene, "Surface micromachined micro opto-electro-mechanical systems," *IEICE Trans. Electron*, pp. 206–213, Feb. 1997.

[4] W. D. Cowan, V. M. Bright, M. K. Lee, and B. M. Welsh, "Evaluation of microfabricated deformable mirror systems," in *Proc. SPIE Conf. Adaptive Optical System Technology*, Kona, HI, Mar. 1998, pp. 790–804.

[5] T. G. Bifano, R. Mali, J. Perreault, K. Dorton, N. Vandelli, M. Horentein, and D. Castanon, "Continuous-membrane surace-micromachined silicon deformable mirror," *Opt. Eng.*, vol. 36, no. 5, p. 1354, 1997.

[6] J. Mansell, P. B. Catrysse, E. K. Gustafson, and R. L. Byer, "Silicon deformable mirrors and CMOS-based wavefront sensors," in *Proc. SPIE Int. Conf. High-Resolution Wavefront Control*, SPIE Int. Soc. Opt. Eng., San Diego, CA, 2000, pp. 15–25.

[7] G. Vdovin, "Optimization-based operation of micromachined deformable mirrors," in *Proc. SPIE Conf. Adaptive Optical System Technology*, Kona, HI, 1998, pp. 902–909.

[8] C. Divoux, J. Charton, W. Schwartz, E. Stadler, J. Margail1, T. E. L. Jocou, J. C. Barbe, J. Chiaroni, and P. Berruyer, "A novel electrostatic actuator for micro deformable mirrors: fabrication and test," in *Proc. IEEE Int. Conf. Solid State Sensors, Actuators, Microsystems*, Boston, MA, 2003, pp. 488–491.

[9] P. Kurczynski, P. Kurczynski, J. A. Tyson, B. Sadoulet, D. Bishop, and D. R. Williams, "Electrostatically actuated membrane mirrors for adaptive optics," in *Proc. SPIE Conf. MOEMS Miniaturized Systems III*, San Jose, CA, 2003, pp. 305–313.

[10] N. Ledermann, A. Seifert, S. Hiboux, and P. Muralt, "Effective transverse piezoelectric coefficient $e_{31,f}$ of (100)/(001) textured PZT thin films," *Integr. Ferroelectr.*, vol. 24, p. 13, 1999.

[11] P. Muralt, A. Kholkin, M. Kohli, and T. Maeder, "Piezoelectric actuation of PZT thin-film diaphragms at static and resonant conditions," *Sens. Actuators A*, vol. 53, p. 398, 1996.

[12] J. Garra, T. Long, J. Currie, T. Schneider, R. White, and M. Paranjapea, "Dry etching of polydimethylsiloxane for microfluidic systems," *J. Vac. Sci. Technol. A*, vol. 20, no. 3, pp. 975–982, May–Jun 2002.

[13] J. A. Perreault, T. G. Bifano, B. M. Levine, and M. N. Horenstein, "Adaptive optic correction using microelectromechanical deformable mirrors," *Opt. Eng.*, vol. 41, no. 3, pp. 561–566, Mar. 2002.

[14] D. Damjanovic, "Stress and frequency dependence of the direct piezoelectric effect in ferroelectric ceramics," *J. Appl. Phys.*, vol. 82, no. 4, pp. 1788–1797, Aug., 15 1997.

[15] T. Bifano, J. A. Perreault, P. A. Bierden, and C. E. Dimas, "Micromachined deformable mirrors for adaptive optics," in *SPIE Conf. High-Resolution Wavefront Control: Methods, Devices, Applications IV*, Seattle, WA, 2002, pp. 10–13.

Yoshikazu Hishinuma received the B.S. degree in applied and engineering physics from Cornell University, Ithaca, NY, in 1997 and the M.S. and Ph.D. degrees in applied physics from Stanford University, Stanford, CA, in 1999 and 2002, respectively.

His thesis research concentrated on experimental and theoretical studies on refrigeration effect of low work function materials during electron tunneling at room temperature. Using his unique experimental setup and technique, he was able to observe the first signature of cooling effect at room temperature. He was with the Jet Propulsion Laboratory, where his main research responsibility was the development of large-area micromachined deformable mirrors using piezoelectric unimorph actuators, targeted for future ultralarge telescopes. He is currently with the Advanced Core Technology Laboratories, Fuji Photo Film Co., Ltd., Japan. His current research interests include microfabrication technologies, adaptive optics, MEMS actuator designs, and sensors for small signal detections.

Eui-Hyeok (EH) Yang (M'03–SM'06) received the B.S., M.S., and Ph.D. degrees from the Department of Control and Instrumentation Engineering, Ajou University, Korea, in 1990, 1992, and 1996, respectively.

He joined the Fujita MEMS research group at the Institute of Industrial Science, University of Tokyo, Japan, as a Visiting Postdoctoral Researcher. He received a research fellowship from the Japan Society for the Promotion of Science from 1996 to 1998. Since 1999, he has been with the Jet Propulsion Laboratory (JPL), Pasadena, CA, where he initiated the development of MEMS adaptive optical devices. He is currently a Senior Member of the Engineering Staff at JPL and the task manager for several MEMS technology development projects. He has extensive experience in MEMS actuator, deformable mirror, and optical membrane fabrication. He is leading the development of MEMS-based deformable mirrors and actuators for future large aperture telescopes. He is also leading the development of MEMS-based piezoelectric valves for future microspacecraft applications. He participated in the technical evaluation of MEMS mirror array technologies being developed for the multiobject spectrometer project for the James Webb Space Telescope. He has successfully developed a membrane-transfer technology for large-area deformable mirrors that is being targeted for ultralarge space telescopes. He has been successful in winning extremely competitive major research grants, which represents an exceptional achievement and productivity within NASA. He is a Technical Monitor for a NASA SBIR project for the development of actuators for optical mirror devices. He has participated in development of several electrostatic, thermopneumatic, piezoelectric, and shape memory alloy devices for microfluidics systems, inertial microsensors, and optical MEMS devices. His current research focuses on microactuators, fluidic microsystems, and adaptive optics for space applications.

Dr. Yang is a Member of the Technical Program Committee (TPC) of the IEEE Sensor Conference and a Member of the Program Committee of the SPIE MOEMS/MEMS Conference. He is also a Topic Organizer of the Micro and Nano Devices Topic of the ASME International Mechanical Engineering Congress and Exposition. He received the Lew Allen Award for Excellence at JPL.